Human Genetics
https://doi.org/10.1007/s00439-021-02296-x

ORIGINAL INVESTIGATION

Chromosomal translocations inactivating *CDKN2A* support a single path for malignant peripheral nerve sheath tumor initiation

Miriam Magallón-Lorenz[1] · Juana Fernández-Rodríguez[2,3,4] · Ernest Terribas[1,13] · Edgar Creus-Batchiller[2,3,4] · Cleofe Romagosa[4,5,6] · Anna Estival[7] · Diana Perez Sidelnikova[8] · Héctor Salvador[9] · Alberto Villanueva[10,3] · Ignacio Blanco[11] · Meritxell Carrió[1] · Conxi Lázaro[2,3,4] · Eduard Serra[1,4] · Bernat Gel[1,12]

Received: 23 March 2021 / Accepted: 24 May 2021

Abstract

Malignant peripheral nerve sheath tumors (MPNST) are aggressive soft tissue sarcomas with poor prognosis, developing either sporadically or in persons with neurofibromatosis type 1 (NF1). Loss of *CDKN2A/B* is an important early event in MPNST progression. However, many reported MPNSTs exhibit partial or no inactivation of *CDKN2A/B*, raising the question of whether there is more than one molecular path for MPNST initiation. We present here a comprehensive genomic analysis of MPNST cell lines and tumors to explore in depth the status of *CDKN2A*. After accounting for *CDKN2A* deletions and point mutations, we uncovered a previously unnoticed high frequency of chromosomal translocations involving *CDKN2A* in both MPNST cell lines and primary tumors. Most identified translocation breakpoints were validated by PCR amplification and Sanger sequencing. Many breakpoints clustered in an intronic 500 bp hotspot region adjacent to *CDKN2A* exon 2. We demonstrate the bi-allelic inactivation of *CDKN2A* in all tumors ($n=15$) and cell lines ($n=8$) analyzed, supporting a single molecular path for MPNST initiation in both sporadic and NF1-related MPNSTs. This general *CDKN2A* inactivation in MPNSTs has implications for MPNST diagnostics and treatment. Our findings might be relevant for other tumor types with high frequencies of *CDKN2A* inactivation.

Eduard Serra and Bernat Gel contributed equally to this work.

✉ Eduard Serra
eserra@igtp.cat

✉ Bernat Gel
bgel@igtp.cat

1 Hereditary Cancer Group, Germans Trias i Pujol Research Institute (IGTP)-PMPPC, Badalona, 08916 Barcelona, Spain

2 Hereditary Cancer Program, Catalan Institute of Oncology (ICO-IDIBELL), L'Hospitalet de Llobregat, 08908 Barcelona, Spain

3 Program in Molecular Mechanisms and Experimental Therapy in Oncology (ONCOBELL), L'Hospitalet de Llobregat, 08908 Barcelona, Spain

4 Centro de Investigación Biomédica en Red de Cáncer (CIBERONC), Barcelona, Spain

5 Pathology Department, Hospital Universitari Vall d'Hebron and Vall d'Hebron Research Institut (VHIR), 08035 Barcelona, Spain

6 Universitat Autònoma de Barcelona, 08193 Bellaterra, Spain

7 B-ARGO Group, Catalan Institute of Oncology - Hospital Universitari Germans Tries i Pujol, Badalona, 08916 Barcelona, Spain

8 Plastic Surgery Service, Functional Sarcoma Unit, ICO-HUB, L'Hospitalet de Llobregat, 08907 Barcelona, Spain

9 Pediatric Oncology Department, Sant Joan de Déu Barcelona Children's Hospital, 08950 Barcelona, Spain

10 Group of Chemoresistance and Predictive Factors, Subprogram Against Cancer Therapeutic Resistance (ProCURE), ICO-IDIBELL, L'Hospitalet del Llobregat, 08908 Barcelona, Spain

11 Programa d'Assessorament i Genètica Clínica, Hospital Universitari Germans Trias i Pujol, Badalona, 08916 Barcelona, Spain

12 Departament de Fonaments Clínics, Universitat de Barcelona, 08036 Barcelona, Spain

13 Present Address: Oncohematology Area, Health Research Institute of the Balearic Islands (IdISBa), Palma de Mallorca, Illes Balears, Spain

Published online: 31 May 2021

Introduction

Malignant peripheral nerve sheath tumors (MPNSTs) are rare malignancies with a peripheral nerve sheath origin. MPNSTs account for 3–10% of all soft tissue sarcomas, being a highly aggressive histological subtype. Approximately half of MPNSTs develop in patients with neurofibromatosis type 1 (NF1) while the other half develop sporadically (Evans 2002; Ferner and Gutmann 2002). The incidence in the general population is 1 per 100,000 (Ducatman et al. 1986; Evans 2002; Carli et al. 2005) and the lifetime risk of an NF1 individual to develop an MPNST is 10–15% (Evans 2002; Uusitalo et al. 2016). Due to its aggressiveness and metastatic potential, MPNSTs constitute a leading cause of death in NF1 (Evans 2002; Ferner and Gutmann 2002; Carli et al. 2005). Like many soft tissue sarcomas, complete resection with wide margins is essential in MPNST therapy, followed by radiation and/or chemotherapy (Porter et al. 2009; Moretti et al. 2011), although standard sarcoma chemotherapy regimens offer limited clinical benefits (Wong et al. 1998).

The diagnosis of MPNSTs can be challenging, especially outside of the NF1 context, since MPNSTs are rare and specific histological criteria have not been completely established (Rodriguez et al. 2012; Le Guellec et al. 2016). In the context of NF1, a common path of MPNST progression is the development of a nodular atypical neurofibroma (aNF) from a pre-existing plexiform neurofibroma (pNF). aNFs are considered premalignant lesions at risk of progression (Beert et al. 2011; Higham et al. 2018). The boundaries for distinguishing a benign pNF from an aNF, and aNF from a low-grade MPNST, are blurry (Beert et al. 2011; Rodriguez et al. 2012; Miettinen et al. 2017). In addition to the loss of *NF1* necessary for pNF formation, aNFs also bear the loss of the *CDKN2A/B* locus (Beert et al. 2011; Röhrich et al. 2016; Carrió et al. 2018; Pemov et al. 2019), although aNF heterogeneity might compromise their detection. In fact, a work studying intra-aNF heterogeneity found distinct histological degrees of atypia and cellularity in the same discrete aNF nodular lesion, correlating with the heterozygous or homozygous inactivation state of *CDKN2A* (Carrió et al. 2018). In mouse models, the loss of *NF1* and *CDKN2A* has been demonstrated to be sufficient to generate an aNF and to predispose to MPNST formation (Rhodes et al. 2019; Chaney et al. 2020).

MPNSTs contain hyperploid and highly rearranged genomes with a low mutation burden (Lee et al. 2014; Brohl et al. 2017; Sohier et al. 2017; Abeshouse et al. 2017). In addition to *NF1* and *CDKN2A/B*, MPNSTs frequently lose components of the polycomb repressive complex 2 (PRC2) (*SUZ12* and *EED*), involved in chromatin remodeling (De Raedt et al. 2014; Zhang et al. 2014; Lee et al. 2014; Cleven et al. 2016; Schaefer et al. 2016; Prieto-Granada et al. 2016). In the pNF-aNF-MPNST progression, *NF1* and *CDKN2A* losses are early events predisposing to MPNST genesis. However, different genomic analyses of MPNSTs evidenced the loss of the *CDKN2A*/B locus in at most 70–80% of MPNST analyzed (Beert et al. 2011; Lee et al. 2014; Röhrich et al. 2016; Lemberg et al. 2020) raising the question of whether there is more than one molecular path for initiating MPNST. There seems to be a constrained order in the acquisition of molecular alterations since pNF only have alterations in *NF1*, aNFs in *NF1* and *CDKN2A* and MPNSTs in these two genes plus in PRC2 genes, among other alterations.

CDKN2A is one of the most commonly inactivated tumor suppressor genes in cancer (Kim and Sharpless 2006; Hamid and Petreaca 2019), although inactivation of *CDKN2A* due to chromosomal translocation is not commonly reported (Hamid and Petreaca 2019). This locus encodes for two proteins $p16^{INK4}$ and $p14^{ARF}$ that regulate two main tumor suppressor pathways, p16/CDK4-6/Rb and p14/MDM2/p53, controlling processes like cell division and senescence, especially in tissue stem cells (Gil and Peters 2006). Loss of *CDKN2A* leads to the higher activation of cyclin-dependent kinases *CDK4/6*, the hyperphosphorylation of retinoblastoma and the induction of S phase, promoting cell division. Different *CDK4/6* inhibitors exist (Palbociclib, Abemaciclib, Ribociclib) currently used in clinical trials for distinct types of tumors and in pre-clinical combination treatments, for instance with MEK inhibitors (Wagner and Gil 2020).

The existence of MPNSTs with and without total inactivation of *CDKN2A*, and its potential implications for molecular-driven diagnostics and therapy, prompted us to perform an exhaustive analysis of the *CDKN2A* locus in a wide range of MPNST cell lines and primary tumors, using different types of genomic analyses.

Materials/subjects and methods

Samples

We analyzed 8 MPNST cell lines, 5 from NF1 patients—ST88-14 (RRID:CVCL_8916), S462 (RRID:CVCL_1Y70), sNF96.2 (RRID:CVCL_K281), NMS-2 (RRID:CVCL_4662), 90-8TL (RRID:CVCL_1B47)—and 3 of sporadic origin—HS-Sch-2 (RRID:CVCL_8718), HS-PSS (RRID:CVCL_8717) and STS-26 T (RRID:CVCL_8917)—and 15 primary MPNSTs, 8 sporadic and 7 from NF1 patients. All patients that provided samples for the study gave their written informed consent.

Tumor processing, DNA and RNA extraction

Tumors were processed and preserved as described elsewhere(Castellsagué et al. 2015; Fernández-Rodríguez et al. 2020) DNA from MPNSTs was extracted using the Gentra Puregene Core Kit A (Qiagen, Hilden, Germany, Cat No. 153667) following the manufacturer's instructions after homogenization using Tissue Lyser (Qiagen, Hilden, Germany). DNA from MPNST cell lines was extracted also using the Gentra Puregene Core Kit A (Qiagen, Hilden, Germany, Cat No. 153667). RNA was extracted using Tripure Isolation Reagent (Roche, Basel, Switzerland, Cat No. 11667157001) according to the manufacturer's instructions. In all cases, the purity and quality of DNA and RNA were assessed using a Nanodrop spectrophotometer, Qubit fluorometer and gel electrophoresis analysis.

SNP-array analysis

SNP-array analysis was performed in 8 MPNST cell lines and 13 primary MPNSTs using Illumina BeadChips (Human660W-Quad, OmniExpress v1.0 and OmniExpress 1.2) at the IGTP High Content Genomics Core Facility. Raw data were processed with Illumina Genome Studio to extract B allele frequency (BAF) and log R ratio (LRR). We used GAP (Popova et al. 2009) to perform copy-number calling.

Whole-exome sequencing

The exome of 8 MPNST cell lines was captured using Agilent SureSelect Human All Exon V5 kit (Agilent, Santa Clara, CA, US) and sequenced in a HiSeq instrument (Illumina, San Diego, CA, US) at Centro Nacional de Analisis Genomicos (CNAG, Barcelona, Spain) to a median of 165.5 million 100 bp paired-end reads per sample. Sequencing reads were then mapped with bwa mem (Li 2013) against GRCh38. We called variants with strelka2 (Kim et al. 2018) and annotated them with annovar (Wang et al. 2010). Pathogenicity of selected *CDKN2A* and *NF1* variants was evaluated using Ensembl's Variant Effect Predictor (VEP).

Whole-Transcriptome sequencing

RNA-seq libraries (TruSeq stranded total RNA, Illumina) of 2 MPNST cell lines (ST88-14, S462) were produced by the IGTP High Content Genomics Core Facility and sequenced in an Illumina HiSeq3000 instrument at CNAG to a median of 74.5 million 150 bp paired-end reads per sample. Sequencing reads were mapped against the GRCh38 genome and Gencode transcriptome using STAR (Dobin et al. 2013).

Whole-genome sequencing

Whole-genome sequencing (WGS) libraries of 2 MPNST cell lines and 9 primary MPSNTs were prepared following standard DNBseq protocols, sequenced in a BGISEQ-500 to a median of 881 million 150 bp paired-end reads per sample and mapped with bwa mem against GRCh38. Small variants were called and evaluated as in WES.

We called copy-number alterations using CNVkit (Talevich et al. 2016) with the recommended settings for WGS data with no matched normal pair (flat reference, difficult region blacklist (https://github.com/Boyle-Lab/Blacklist/blob/master/lists/hg38-blacklist.v2.bed.gz), -no-edge option and 1000 bp bins). To obtain the exact copy number profile of each sample we used the threshold method with sample-specific thresholds defined taking into account sample purity computed from loss-of-heterozygosity (LOH) regions in SNP-array data.

We used two structural variant (SV) callers: LUMPY (Layer et al. 2014) via smoove (https://github.com/brentp/smoove) with parameters for small-cohorts and excluding the problematic regions defined in https://github.com/hall-lab/speedseq/blob/master/annotations/exclude.cnvnator_100bp.GRCh38.20170403.bed and MANTA (Chen et al. 2016) with parameters for tumor-only analysis. Only SV break-ends called by both tools were deemed valid.

Visualization

Visual inspection of NGS data was performed in the Integrative Genomics Viewer (IGV). Genomic plots were created using karyoploteR (Gel and Serra 2017) and CopyNumberPlots (Gel and Magallón-Lorenz 2019) R packages and circular genome representations with Circos (Connors et al. 2009).

Breakpoint validation

Inter-chromosomal rearrangements detected by LUMPY and MANTA in *CDKN2A* were validated by PCR and Sanger sequencing. The PCR primers designed flanking *CDKN2A/B* breakpoints, annealing temperatures used and amplicon lengths are summarized in Supp Table 3.

Results

CDKN2A inactivation in MPNST cell lines

CDKN2A is one of the most commonly inactivated tumor suppressor genes in cancer (Kim and Sharpless 2006; Hamid

and Petreaca 2019) and a key player in MPNST-genesis (Beert et al. 2011). To investigate the status of *CDKN2A* in MPNSTs we analyzed 8 established MPNST cell lines, including 5 NF1-associated and 3 of sporadic origin. We first performed SNP-array and whole-exome sequencing (WES) on all of them to identify those with only one *CDKN2A* allele inactivated or with no apparent alteration of *CDKN2A*. Copy-number calling on SNP-array data showed homozygous deletions affecting the *CDKN2A/B* locus in 3 cell lines (90–8-TL, sNF96.2, HS-PSS) (Fig. 1A, B). 90–8-TL and sNF96.2 presented a single deletion combined with the loss-of-heterozygosity (LOH) of the whole chromosome arm, while HS-PSS presented two independent overlapping deletions. Two other cell lines showed heterozygous deletions (NMS-2, S462). WES data showed a homozygous damaging missense variant in STS-26 T affecting *CDKN2A* exon 2 (Fig. 1B; Supp. Table 1; Supp. Fig. 1). Thus, after accounting for deletions and point mutations, in four out of eight cell lines (ST88-14, HS-Sch-2, NMS-2, S462) at least one copy of *CDKN2A* remained apparently intact.

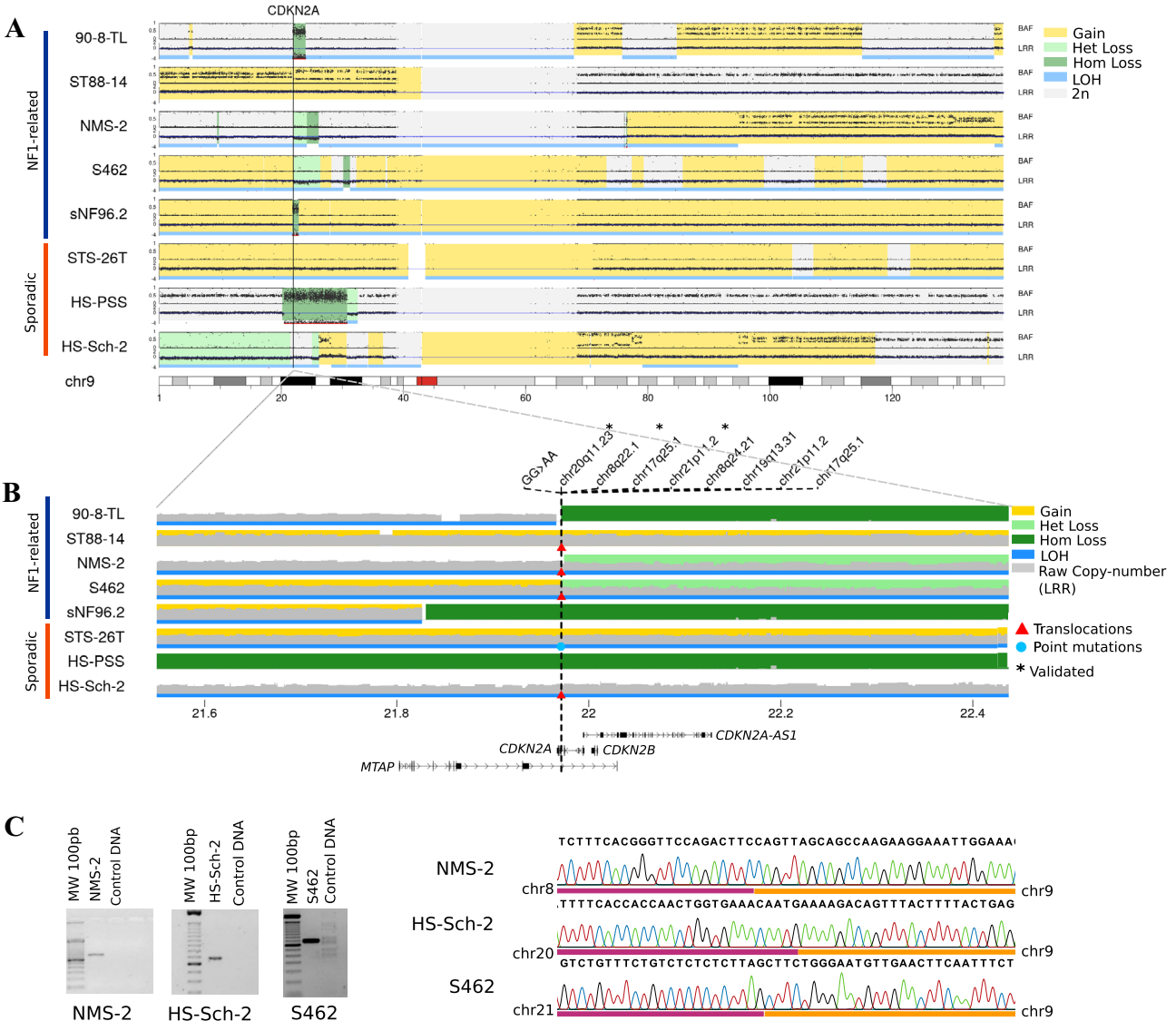

Fig. 1 Status of the *CDKN2A/B* genomic region in MPNST cell lines. A SNP-array raw data of the whole chromosome 9 of 8 MPNST cell lines: B-allele frequency (BAF), Log R-ratio (LRR), copy-number alterations (colored regions) and loss-of-heterozygosity (LOH, blue line) are shown. **B** Closer view of the CDKN2A/B region showing LRR (grey area), copy-number alterations and LOH (colored regions and blue line) from SNP-array analysis; and translocation breakpoints (red triangles and black vertical lines) and point mutations (blue dots) from WES and RNA-seq analysis. **C** Validation by PCR and Sanger sequencing of three translocation breakpoints identified on WES and RNA-seq data

Unexpectedly, further careful visual inspection of WES data revealed the presence of a cluster of soft-clipped reads, reads with ends that are unmappable to the reference sequence, in an intronic region adjacent to *CDKN2A* exon 2 in ST88-14, HS-Sch-2 and NMS-2 cell lines (Supp. Fig. 2). In each cell line, soft-clipped reads had their mates in a different chromosome (Supp. Fig. 2), indicating potential translocation events with different partners. For HS-Sch-2 and NMS-2 cell lines, all reads spanning the potential translocation breakpoint were soft-clipped, indicating a homozygous event consistent with the LOH identified by SNP-array. We validated two of the three identified translocation breakpoints by PCR amplification and Sanger sequencing (HS-Sch-2, NMS-2) (Fig. 1C). For the ST88-14 cell line, the breakpoint was localized to a highly repetitive region hindering its PCR amplification.

At this point, we had detected the bi-allelic inactivation of *CDKN2A* in all cell lines but two, S462 and ST88-14, where only partial inactivation of *CDKN2A* was detected. For these two cell lines, we performed RNA-seq analysis. ST88-14 presented an altered coverage pattern, but we were not able to identify any structural variant breakpoint. Visual inspection of S462 RNA-seq data of this locus revealed an accumulation of soft-clipped reads with their mate in a different chromosome, pointing again to a translocation event in the same intronic region, although further inside the intron and thus not covered by WES reads (Supp. Fig. 3). We used PCR and Sanger sequencing to validate the translocation (Fig. 1C).

To obtain further evidence of the complete inactivation of the locus, we designed PCR primers flanking the region containing all translocation breakpoints identified and tested all 8 cell lines. None of the samples showed an amplification signal, except the STS-26 T cell line, the one bearing a *CDKN2A* point mutation in homozygosity (Supp. Fig. 4B).

This result prompted us to further analyze the ST88-14 and S462 cell lines by whole genome sequencing (WGS) to investigate other potential alterations in *CDKN2A*. WGS validated the translocations identified in both cell lines and revealed additional translocations affecting the same region but farther from the exon boundary, explaining why WES analysis was not able to identify them. Interestingly, all translocation breakpoints clustered in a 500 bp intronic region, representing a translocation hotspot (Supp. Fig. 4A). In S462 we identified two homozygous translocations separated by a small 177 bp homozygous deletion (Supp. Fig. 5), one of them sharing the breakpoint with the heterozygous deletion previously identified (Fig. 1A) in SNP-array, consistent with the whole chromosome LOH observed by SNP-array. In ST88-14 we identified two nested heterozygous deletions flanked by translocation breakpoints disrupting both alleles (Supp. Fig. 5). The deletions identified by WGS were small, 87 and177 bp, which is well below the resolution of SNP-arrays and explains why these deletions were missed in the first analysis.

Taking together all the mutations identified (deletions, point mutations and translocations), our analysis confirmed the bi-allelic inactivation of *CDKN2A* in all the MPNST cell lines tested (Table 1).

CDKN2A inactivation in primary MPNSTs

Since results analyzing MPNST cell lines showed the complete inactivation of the *CDKN2A* locus in all cases, we decided to determine if the same was true for primary MPNSTs. To this end, we performed copy-number calling on SNP-array data from 13 primary tumors (Fig. 2). We detected the complete deletion of *CDKN2A* in seven of these. Of the remaining six, four showed a copy-number change within *CDKN2A* itself, suggesting a potential breakpoint in the gene body, and two showed only copy-neutral LOH in the *CDKN2A* region.

To further investigate other alterations affecting *CDKN2A,* we selected seven primary MPNSTs for whole-genome sequencing (WGS) (labeled with a star in Fig. 2): all six MPNSTs with no clear homozygous deletion of the whole locus, plus one tumor where the locus was deleted in homozygosis (MPNST-NF-08). We performed WGS of these 7 primary MPNSTs plus 2 additional tumors for which we did not have SNP-array data (MPNST-NF-13, MPNST-SP-10), for a total of nine primary MPNST, four sporadic and five NF1-related.

Copy-number analysis of WGS data identified all deletions involving the *CDKN2A/B* region identified on SNP-array. However, there were differences between the two technologies. The most important of which was a potential SNP-array copy-number overestimation in different samples including the two tumors with CN-LOH in the *CDKN2A* region (MPNST-SP-02 and MPNST-SP-08), which contained a heterozygous deletion of the region according to WGS data. In total, we identified four heterozygous and five homozygous deletions of the *CDKN2A* region on WGS data (Supp. Fig. 6). Structural variant calling identified a large number of alterations in the *CDKN2A/B* region (Fig. 3A, B) including seven translocation breakpoints in four MPNSTs. In fact, some of the identified focal deletions were caused by inversions and translocations (e.g. MPNST-NF-09, MPNST-NF-10) (Supp. Document 1). Most *CDKN2A* breakpoints (4/7) occurred in the 500-bp translocation hotspot we identified next to *CDKN2A* exon 2 (Figs. 3B, 4). We performed a sequence analysis of this region but we were not able to identify any particular motif or element that could be associated with its susceptibility to break (Supp. Fig. 7). WGS also facilitated the identification of translocation breakpoints away from this region (Figs. 3A, B and 4B). We selected at least one translocation breakpoint located in *CDKN2A* per

Table 1 Summary of allelic inactivation of *CDKN2A* in MPNST and MPNST cell lines

SAMPLE		Allele 1	Allele 2	Inactivation
NF1-associated Tumor	MPNST-NF-03	Deletion	LOH	Complete
	MPNST-NF-04	Deletion	LOH	Complete
	MPNST-NF-08*	Inversion-mediated deletion	Translocation-mediated deletion	Complete
	MPNST-NF-09*	Inversion-mediated deletion	Deletion	Complete
	MPNST-NF-10*	Translocation mediated deletion	Deletion	Complete
	MPNST-NF-12*	Translocation-mediated deletion	Translocation-mediated deletion	Complete
	MPNST-NF-13*	Translocation-mediated deletion	Deletion	Complete
Sporadic Tumor	MPNST-SP-02*	Deletion	Deletion	Complete
	MPNST-SP-03	Deletion	LOH	Complete
	MPNST-SP-04*	Translocation-mediated deletion	Translocation-mediated deletion	Complete
	MPNST-SP-05	Deletion	LOH	Complete
	MPNST-SP-06	Deletion	LOH	Complete
	MPNST-SP-07	Deletion	LOH	Complete
	MPNST-SP-08*	Translocation-mediated deletion	Point mutation	Complete
	MPNST-SP-10*	Deletion	LOH	Complete
NF1-associated Cell line	ST88-14*	Translocation-mediated deletion	Translocation-mediated deletion	Complete
	NMS-2	Translocation	LOH	Complete
	sNF96.2	Deletion	LOH	Complete
	S462*	Translocation	LOH	Complete
	90-8TL	Deletion	LOH	Complete
Sporadic Cell line	STS-26 T	Point mutation	LOH	Complete
	HS-Sch-2	Translocation	LOH	Complete
	HS-PSS	Deletion	Deletion	Complete

*Analysis based on WGS data

sample (Fig. 3B) and validated them by PCR and Sanger sequencing (Fig. 3C). As we observed for MPNST cell lines, all breakpoints in primary MPNSTs had translocation partners in different chromosomes (Figs. 3C, 4A), indicating no preference for a translocation partner and suggesting a non-directed random process inactivating *CDKN2A*.

Finally, one tumor (MPNST-SP-08) had a frameshift deletion of two nucleotides in *CDKN2A* exon 2 (Supp. Fig. 8). Like the homozygous point mutation inactivating *CDKN2A* in the STS-26 T cell line, this point mutation was in the coding region of *CDKN2A* exon 2, in a region shared by the two proteins encoded by this gene, $p16^{INK4}$ and $p14^{ARF}$.

WGS results confirmed the bi-allelic inactivation of *CDKN2A* in all nine MPNSTs studied (Table 1, Supp. Table 1 and Supp. Document 1), and considering results from SNP-array and WGS analyses together, all 15 primary MPNSTs analyzed bore the complete inactivation of the *CDKN2A* tumor suppressor gene (Table 1).

Finally, in the context of NF1 all PNS tumors bear the double inactivation of *NF1* and aNF, the pre-malignant tumors, bear both *NF1* and *CDKN2A* inactivated, highlighting these two genes as early events in MPNST genesis. We also analyzed the *NF1* region from WGS data on sporadic MPNSTs. This analysis revealed that *NF1* was also inactivated in most of them (3 out of 4 sequenced sporadic MPNSTs), including one inactivation caused by a translocation and one by an inversion (Supp. Table 2), and reinforcing the importance of these two genes as crucial initial events for an MPNST to form.

Discussion

In the framework of NF1, the progression pNF-aNF-MPNST is well established as a general path of MPNST initiation, at the histological level (McCarron and Goldblum 1998; Miettinen et al. 2017) and because in benign–malignant progressions, pNF or aNF and MPNST share the same *NF1* somatic mutation (Beert et al. 2011; Hirbe et al. 2015). Advanced aNFs bear the double inactivation of *NF1* and *CDKN2A* (Carrió et al. 2018). However, not all reported MPNSTs had *CDKN2A* totally inactivated, some exhibiting a heterozygous loss and others no involvement at all (Lee et al. 2014; Röhrich et al. 2016), opening up the possibility of MPNST genesis without *CDKN2A* participation, and its potential implications for molecular-driven diagnostics and therapy. In this context, we began a comprehensive analysis

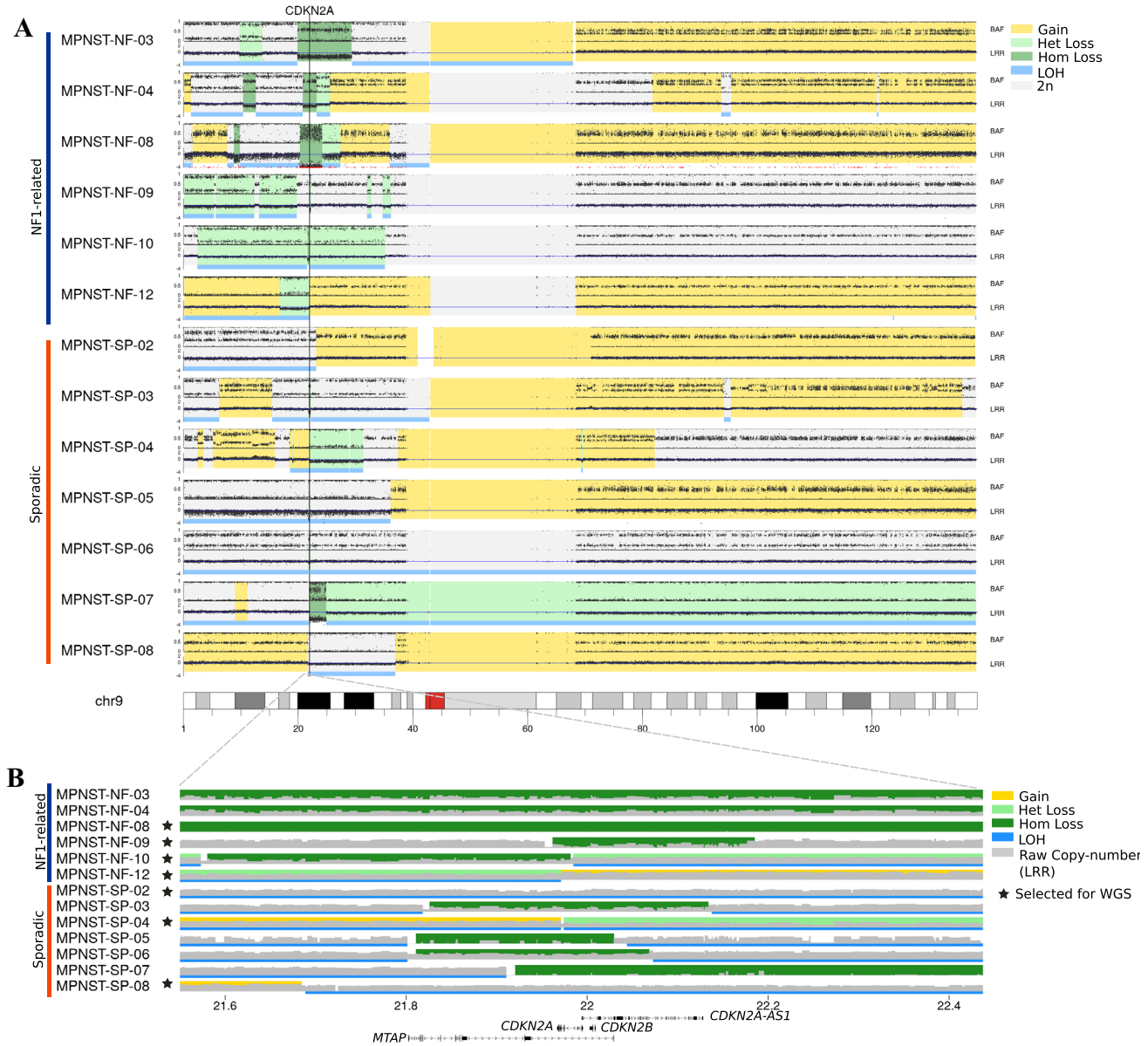

Fig. 2 Status of the *CDKN2A/B* genomic region in primary MPNSTs based on SNP-array. **A** SNP-array raw data of the whole chromosome 9 of 15 MPNST primary tumors: B-allele frequency (BAF), Log R-ratio (LRR), copy-number alterations (colored regions) an loss-of-heterozygosity (LOH, blue line) are shown. **B** Closer view of the *CDKN2A/B* region with LRR (grey area), copy-number alterations (colored regions) and LOH (blue line). Samples with a star (★) were selected for WGS

of *CDKN2A*, applying different types of genomic analyses, in a wide range of MPNST cell lines and primary tumors.

To our surprise, after accounting for deletions and point mutations, we identified, for the first time, a high frequency of chromosomal translocations involving *CDKN2A* (Fig. 3), many of them (11 out of 15) located in an intronic hotspot of 500 bp, close to *CDKN2A* exon 2. *CDKN2A* is one of the most frequently inactivated genes not only in MPNSTs but also in cancer in general (Kim and Sharpless 2006; Hamid and Petreaca 2019), although chromosomal translocation has not been commonly reported as an inactivating mechanism (Hamid and Petreaca 2019). In our case, WGS was key to identify all possible translocations in the *CDKN2A/B* region, even those not involving the hotspot identified. Its limited use in the study of MPNST genomes (Zhang et al. 2014) may explain why this high frequency of translocations has been missed. Only a careful examination of sequencing reads and the proximity of the identified breakpoint hotspot to *CDKN2A* exon 2 allowed the identification of these translocations from

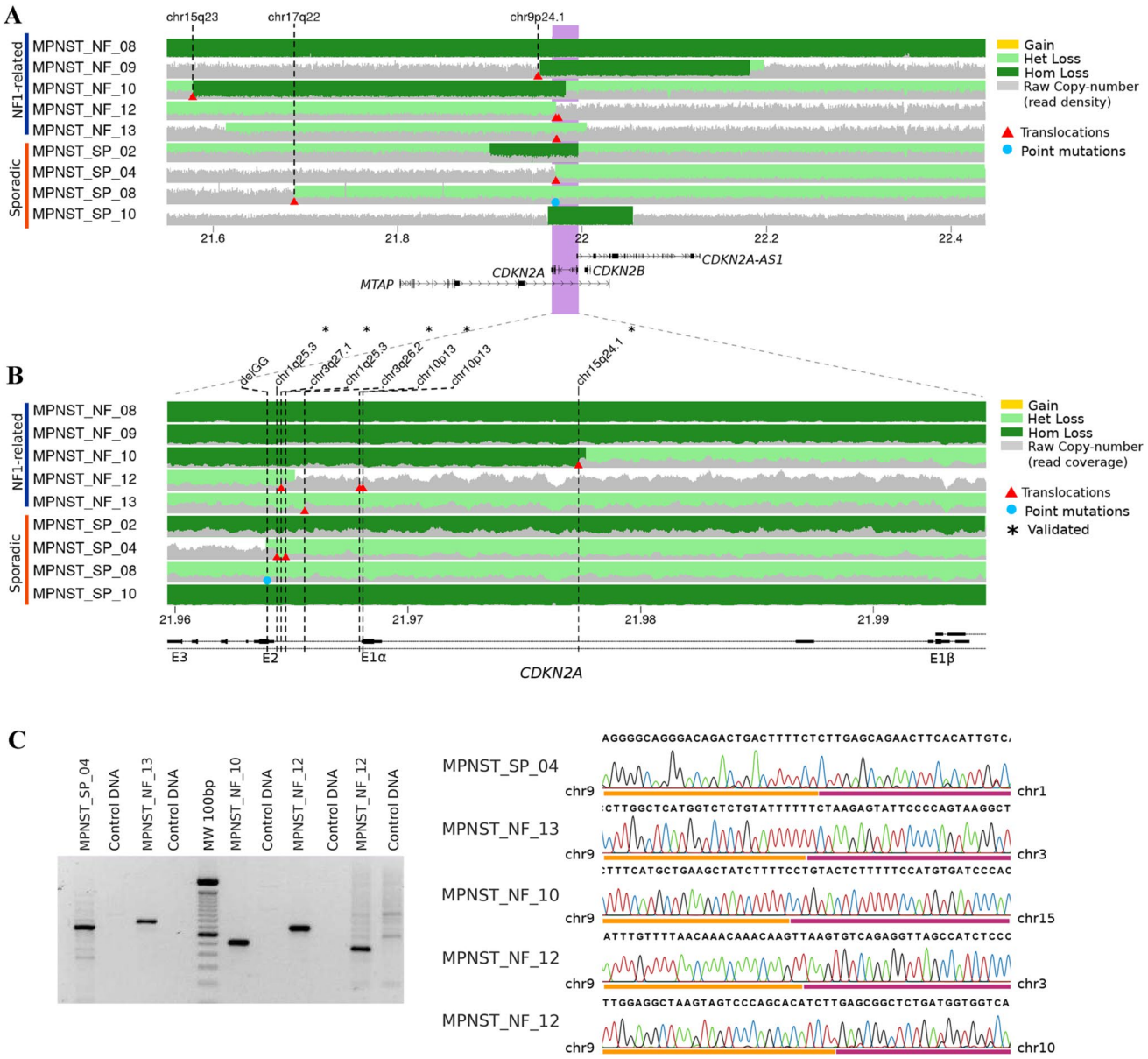

Fig. 3 Status of the *CDKN2A/B* genomic region in primary MPNSTs based on WGS. **A** WGS-based copy number analysis of MPNSTs showing read density (grey area), copy-number alterations (colored areas), translocation breakpoints (red triangles and black vertical lines) and point mutations (blue dots). Translocations overlapping the *CDKN2A* gene (purple shaded region) are shown only with a red triangle in this general view. **B** Closer view of the *CDKN2A* locus. Here the grey area represents WGS read coverage. **C** Validation by PCR and Sanger sequencing of five translocation breakpoints

WES and RNA-seq data. The absence of reported translocations affecting *CDKN2A* in other tumor types could indicate a different mechanism of inactivation, a lower involvement of *CDKN2A* inactivation, and/or the lack of sufficient WGS. We think that the higher frequency of chromosomal translocations affecting *CDKN2A* identified may also occur in other tumor types in which *CDKN2A* is frequently inactivated (other sarcomas, tumors with a neural crest related origin, gliomas, …)(Kim and Sharpless 2006; Hamid and Petreaca 2019).

In the context of NF1, *CDKN2A* inactivation occurs at the level of aNF before MPNST formation, as a necessary molecular event for malignant progression from this pre-malignant state, and conferring MPNST predisposition (Beert et al. 2011; Rhodes et al. 2019; Chaney et al. 2020). In fact, some of the identified *CDKN2A* copy number losses in aNFs contain its breakpoints within the locus (Carrió et al. 2018; Pemov et al. 2019), suggesting a translocation event. Our results strongly support that loss of *CDKN2A* is also a necessary step for sporadic MPNST formation. In

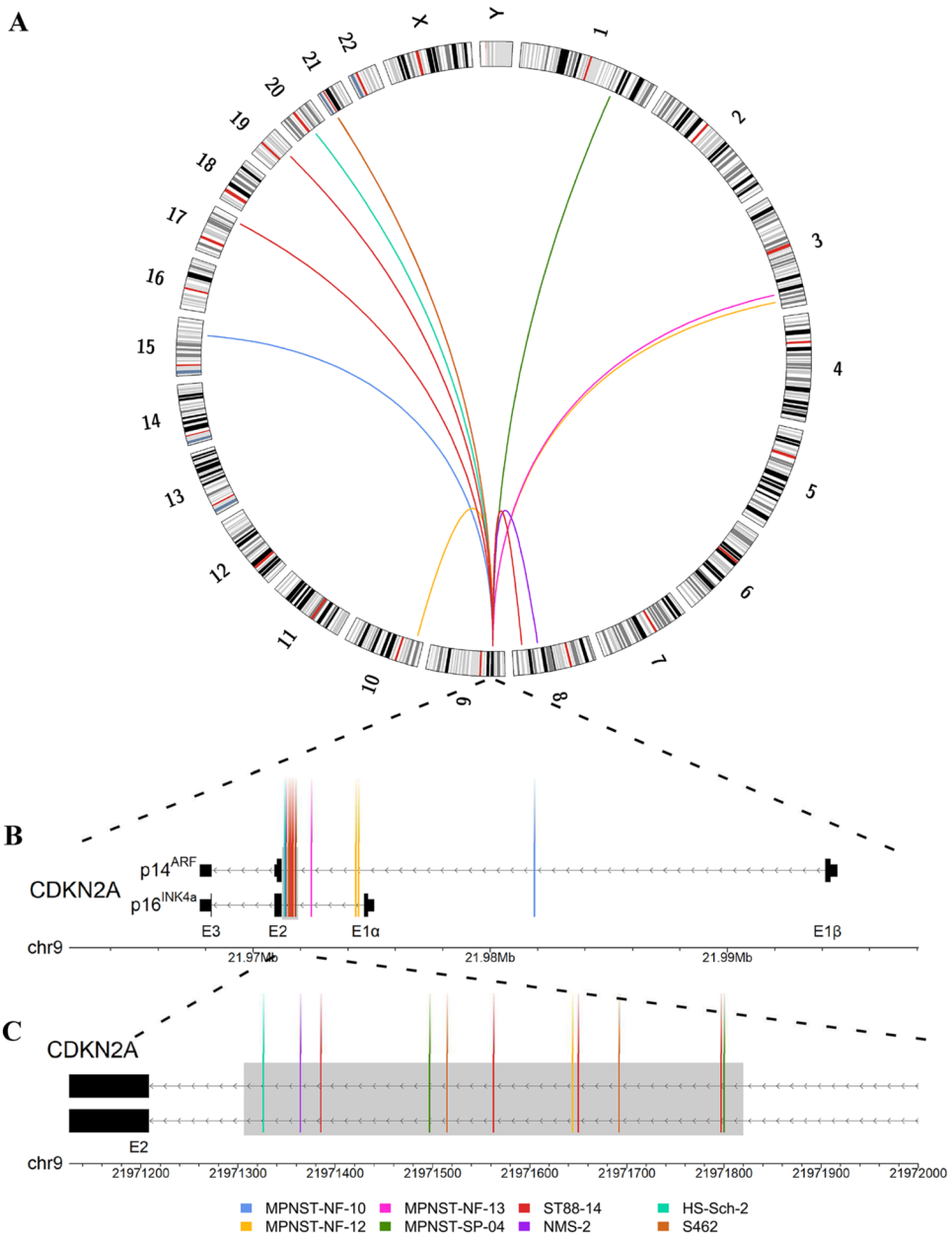

Fig. 4 Summary of translocation breakpoints in *CDKN2A* identified in MPNST tumors and cell lines. **A** Circos plot showing all 15 translocation breakpoint detected in *CDKN2A* and their translocation partners. On this broad view, only 11 lines are visible due to overlaps. **B** Closer view of the *CDKN2A* locus containing all 15 translocation events. **C** Zoom into the translocation hotspot (shaded in gray) next to *CDKN2A* exon 2 containing 11 of the breakpoints

fact, we also identified the inactivation of the *NF1* gene in three out of four sporadic MPNST sequenced, in line with previous reports (Lee et al. 2014). However, knowledge from the NF1 condition points to a view of MPNST genesis as a constrained ordered sequence of genetic events. For instance, PRC2 is never altered in aNF (Beert et al. 2011; Röhrich et al. 2016; Carrió et al. 2018; Pemov et al. 2019), contrasting with MPNSTs in which it is one of the most frequently lost loci (De Raedt et al. 2014; Zhang et al. 2014; Lee et al. 2014; Cleven et al. 2016; Schaefer et al. 2016; Prieto-Granada et al. 2016). In addition, NF1 patients bearing microdeletions involving *NF1* and *SUZ12* genes, develop a high number of cutaneous neurofibromas, never progressing towards MPNST and never exhibiting LOH as a somatic inactivating mechanism (De Raedt et al. 2006; Maertens et al. 2006), as if a double inactivation of *NF1* and PRC2 was not viable without losing *CDKN2A* first.

The high number of translocations detected in the *CDKN2A/B* locus (some MPNSTs presented up to four translocations in the region) indicates a high instability of this complex locus in the cell originating an MPNST. We are not sure whether other coding or non-coding elements of the *CDKN2A/B* region might be involved in MPNST formation. The fact that most alterations are caused by large deletions or translocations and few by point mutations in *CDKN2A*, favors the view of a multiple functional impact of these alterations. On the other hand, the identification of point mutations altering only $p16^{INK4}$ and $p14^{ARF}$ opens

up the possibility that only the loss of these two proteins is sufficient for MPNST genesis and that the high frequency of large alterations is just pointing to the most likely mechanism of inactivation. So far, we can assure that a comprehensive genomic analysis of this region demonstrates the necessary complete inactivation of *CDKN2A* for MPNST formation.

The diagnosis of MPNSTs based on imaging and pathology analysis can be challenging (Rodriguez et al. 2012; Le Guellec et al. 2016) and a clear understanding of the molecular alterations present in MPNSTs might help in this regard. A careful genomic analysis of *CDKN2A* status in combination with other genetic alterations might provide an additional piece of information for a differential diagnostic, either from aNF or from other soft tissue sarcomas. In addition, loss of *CDKN2A* leads to the higher activation of cyclin-dependent kinases *CDK4/6*, contributing to a cancer cell state. Different *CDK4/6* inhibitors exist and are currently being used in clinical trials for distinct types of tumors and in pre-clinical combination treatments, for instance with MEK inhibitors (Wagner and Gil 2020). Thus, the loss of *CDKN2A* may not only help MPNST diagnostics but could offer the possibility of using *CDK4/6* inhibitors, in combination with other agents, as a potentially effective therapy on all MPNSTs.

Conclusions

Our work identified the complete inactivation of *CDKN2A* in all MPNSTs ($n=15$) and MPNST cell lines ($n=8$) analyzed. These results strongly support that the complete loss of *CDKN2A* is necessary for MPNST development, favoring a model of a single molecular path in the first steps of MPNST genesis, regardless of its development in a sporadic or NF1 context. We have identified that a substantial percentage of *CDKN2A* inactivation in MPNSTs is due to translocations between *CDKN2A* and other unrelated regions of the genome, many of them with a breakpoint located in an intronic hotspot of 500 bp close to exon 2 of the gene. This mechanism might be relevant in other types of tumors with high frequencies of *CDKN2A* inactivation. These findings also have implications for the molecular-driven diagnostics and treatment of MPNSTs. The identification of this generalized inactivation of *CDKN2A* in MPNSTs may foster the use of *CDK4/6* inhibitors in combination with other agents for MPNST treatment.

Supplementary Information The online version contains supplementary material available at https://doi.org/10.1007/s00439-021-02296-x.

Acknowledgements We thank all patients that participated in this study and provided samples. We would like to thank Álex Negro, Elisabeth Castellanos, Inma Rosas and Helena Mazuelas for their technical support and scientific discussions. We would like to thank the constant support of the NF lay associations: Asociación de Afectados de Neurofibromatosis and ACNefi.

Author contributions Conceptualization: MM-L, BG and ES; Software, formal analysis and visualization: MM-L and BG; Investigation and validation: MM-L; Resources: JF-R, ET, EC-B, CR, AE, DPS, HS, AV, IB, MC and CL; Writing—original draft: MM-L, BG and ES; Writing—review and editing: MM-L, BG and ES; Supervision: ES and BG; Funding acquisition: BG, ES and CL.

Funding This work has been supported by the Instituto de Salud Carlos III National Health Institute funded by FEDER funds—a way to build Europe—[PI14/00577, PI17/00524, PI19/00553, PI20/00228]; Fundación PROYECTO NEUROFIBROMATOSIS (projects to CL and BG-ES); the Government of Catalonia [2017-SGR-496], CERCA Program; Fundació La Marató de TV3 (51/C/2019). MM-L and EC-B are supported by Fundación PROYECTO NEUROFIBROMATOSIS. CR is supported by a grant from the "Programa d'impuls del talent i de l'ocupabilitat del PERIS 2016-2020".

Data availability Genomic data from cell lines (SNP-array, RNA-seq and WES) has been deposited in Synapse (https://www.synapse.org/, syn22392179) and is accessible as part of the NF Data Portal with no access restrictions. Patient-derived WGS data is available at the European Genotype–Phenotype Archive (EGA) (EGAS00001004658) and is available under a data usage agreement.

Declarations

Conflict of interest The authors declare no competing interests.

Ethical approval This work has been approved by the Germans Trias i Pujol Hospital (HUGTiP) Ethics Committee.

Consent to participate All patients gave their written informed consent.

References

Abeshouse A, Adebamowo C, Adebamowo SN et al (2017) Comprehensive and integrated genomic characterization of adult soft tissue sarcomas. Cell 171:950-965.e28. https://doi.org/10.1016/j.cell.2017.10.014

Beert E, Brems H, Daniëls B et al (2011) Atypical neurofibromas in neurofibromatosis type 1 are premalignant tumors. Genes Chromosom Cancer 50:1021–1032. https://doi.org/10.1002/gcc.20921

Brohl AS, Kahen E, Yoder SJ et al (2017) The genomic landscape of malignant peripheral nerve sheath tumors: diverse drivers of ras pathway activation. Sci Rep 7:1–5. https://doi.org/10.1038/s41598-017-15183-1

Carli M, Ferrari A, Mattke A et al (2005) Pediatric malignant peripheral nerve sheath tumor: the italian and german soft tissue sarcoma cooperative group. J Clin Oncol 23:8422–8430. https://doi.org/10.1200/JCO.2005.01.4886

Carrió M, Gel B, Terribas E et al (2018) Analysis of intratumor heterogeneity in Neurofibromatosis type 1 plexiform neurofibromas and neurofibromas with atypical features: correlating histological

and genomic findings. Hum Mutat 39:1112–1125. https://doi.org/10.1002/humu.23552
Castellsagué J, Gel B, Fernández-Rodríguez J et al (2015) Comprehensive establishment and characterization of orthoxenograft mouse models of malignant peripheral nerve sheath tumors for personalized medicine. EMBO Mol Med 7:608–627. https://doi.org/10.15252/emmm.201404430
Chaney KE, Perrino MR, Kershner LJ et al (2020) Cdkn2a loss in a model of neurofibroma demonstrates stepwise tumor progression to atypical neurofibroma and MPNST. Cancer Res 80:4720–4730. https://doi.org/10.1158/0008-5472.CAN-19-1429
Chen X, Schulz-Trieglaff O, Shaw R et al (2016) Manta: rapid detection of structural variants and indels for germline and cancer sequencing applications. Bioinformatics 32:1220–1222. https://doi.org/10.1093/bioinformatics/btv710
Cleven AHG, Al Sannaa GA, Briaire-de Bruijn I et al (2016) Loss of H3K27 tri-methylation is a diagnostic marker for malignant peripheral nerve sheath tumors and an indicator for an inferior survival. Mod Pathol 29:582–590. https://doi.org/10.1038/modpathol.2016.45
Connors J, Krzywinski M, Schein J et al (2009) Circos: an information aesthetic for comparative genomics. Genome Res 19:1639–1645. https://doi.org/10.1101/gr.092759.109.19
De Raedt T, Maertens O, Chmara M et al (2006) Somatic loss of wild type NF1 allele in neurofibromas: comparison of NF1 microdeletion and non-microdeletion patients. Genes Chromosom Cancer 45:893–904. https://doi.org/10.1002/gcc.20353
De Raedt T, Beert E, Pasmant E et al (2014) PRC2 loss amplifies Ras-driven transcription and confers sensitivity to BRD4-based therapies. Nature 514:247–251. https://doi.org/10.1038/nature13561
Dobin A, Davis CA, Schlesinger F et al (2013) STAR: Ultrafast universal RNA-seq aligner. Bioinformatics 29:15–21. https://doi.org/10.1093/bioinformatics/bts635
Ducatman BS, Scheithauer BW, Piepgras DG et al (1986) Malignant peripheral nerve sheath tumors. A clinicopathologic study of 120 cases. Cancer 57:2006–2021. https://doi.org/10.1002/1097-0142(19860515)57:10%3c2006::AID-CNCR2820571022%3e3.0.CO;2-6
Evans DG (2002) MPNST in NF1. J Med Genet 39:311–314
Fernández-Rodríguez J, Morales La Madrid A, Gel B et al (2020) Use of patient derived orthotopic xenograft models for real-time therapy guidance in a pediatric sporadic malignant peripheral nerve sheath tumor. Ther Adv Med Oncol 12:1–11. https://doi.org/10.1177/1758835920929579
Ferner RE, Gutmann DH (2002) International consensus statement on malignant peripheral nerve sheath tumors in neurofibromatosis. Cancer Res 62:1573–1577
Gel B, Magallón-Lorenz M (2019) CopyNumberPlots: Create Copy-Number Plots using karyoploteR functionality. R package version 1.6.0. https://doi.org/10.18129/B9.bioc.CopyNumberPlots
Gel B, Serra E (2017) karyoploteR: an R/Bioconductor package to plot customizable genomes displaying arbitrary data. Bioinformatics 33:3088–3090. https://doi.org/10.1093/bioinformatics/btx346
Gil J, Peters G (2006) Regulation of the INK4b-ARF-INK4a tumour suppressor locus: all for one or one for all. Nat Rev Mol Cell Biol 7:667–677. https://doi.org/10.1038/nrm1987
Hamid MA, Petreaca R (2019) Frequent homozygous deletions of the CDKN2A locus in somatic cancer tissues. Mutat Res Mol Mech Mutagen 815:30–40. https://doi.org/10.1016/j.mrfmmm.2019.04.002
Higham CS, Dombi E, Rogiers A et al (2018) The characteristics of 76 atypical neurofibromas as precursors to neurofibromatosis 1 associated malignant peripheral nerve sheath tumors. Neuro Oncol 20:818–825. https://doi.org/10.1093/neuonc/noy013
Hirbe AC, Dahiya S, Miller CA et al (2015) Whole exome sequencing reveals the order of genetic changes during malignant transformation and metastasis in a single patient with NF1-plexiform neurofibroma. Clin Cancer Res 21:4201–4211. https://doi.org/10.1158/1078-0432.CCR-14-3049
Kim WY, Sharpless NE (2006) The regulation of INK4/ARF in cancer and aging. Cell 127:265–275. https://doi.org/10.1016/j.cell.2006.10.003
Kim S, Scheffler K, Halpern AL et al (2018) Strelka2: fast and accurate calling of germline and somatic variants. Nat Methods 15:591–594. https://doi.org/10.1038/s41592-018-0051-x
Layer RM, Chiang C, Quinlan AR, Hall IM (2014) LUMPY: a probabilistic framework for structural variant discovery. Genome Biol 15:R84. https://doi.org/10.1186/gb-2014-15-6-r84
Le Guellec S, Decouvelaere A-V, Filleron T et al (2016) Malignant peripheral nerve sheath tumor is a challenging diagnosis: a systematic pathology review, immunohistochemistry, and molecular analysis in 160 patients from the french sarcoma group database. Am J Surg Pathol 40:896–908. https://doi.org/10.1097/PAS.0000000000000655
Lee W, Teckie S, Wiesner T et al (2014) PRC2 is recurrently inactivated through EED or SUZ12 loss in malignant peripheral nerve sheath tumors. Nat Genet 46:1227–1232. https://doi.org/10.1038/ng.3095
Lemberg KM, Wang J, Pratilas CA (2020) From genes to -omics: the evolving molecular landscape of malignant peripheral nerve sheath tumor. Genes (basel) 11:691. https://doi.org/10.3390/genes11060691
Li H (2013) Aligning sequence reads , clone sequences and assembly contigs with BWA-MEM. arXiv:1303.3997
Maertens O, Brems H, Vandesompele J et al (2006) Comprehensive NF1 screening on cultured Schwann cells from neurofibromas. Hum Mutat 27:1030–1040. https://doi.org/10.1002/humu.20389
McCarron KF, Goldblum JR (1998) Plexiform neurofibroma with and without associated malignant peripheral nerve sheath tumor: a clinicopathologic and immunohistochemical analysis of 54 cases. Mod Pathol 11:612–617
Miettinen MM, Antonescu CR, Fletcher CDM et al (2017) Histopathologic evaluation of atypical neurofibromatous tumors and their transformation into malignant peripheral nerve sheath tumor in patients with neurofibromatosis 1—a consensus overview. Hum Pathol 67:1–10. https://doi.org/10.1016/j.humpath.2017.05.010
Moretti VM, Crawford EA, Staddon AP et al (2011) Early outcomes for malignant peripheral nerve sheath tumor treated with chemotherapy. Am J Clin Oncol Cancer Clin Trials 34:417–421. https://doi.org/10.1097/COC.0b013e3181e9c08a
Pemov A, Hansen NF, Sindiri S et al (2019) Low mutation burden and frequent loss of CDKN2A/B and SMARCA2, but not PRC2, define premalignant neurofibromatosis type 1–associated atypical neurofibromas. Neuro Oncol 21:981–992. https://doi.org/10.1093/neuonc/noz028
Popova T, Manié E, Stoppa-Lyonnet D et al (2009) Genome alteration print (GAP): a tool to visualize and mine complex cancer genomic profiles obtained by SNP arrays. Genome Biol 10:R128. https://doi.org/10.1186/gb-2009-10-11-r128
Porter DE, Prasad V, Foster L et al (2009) Survival in malignant peripheral nerve sheath tumours: a comparison between sporadic and neurofibromatosis type 1-associated tumours. Sarcoma. https://doi.org/10.1155/2009/756395
Prieto-Granada CN, Wiesner T, Messina JL et al (2016) Loss of H3K27me3 expression is a highly sensitive marker for sporadic and radiation-induced MPNST. Am J Surg Pathol 40:479–489. https://doi.org/10.1097/PAS.0000000000000564
Rhodes SD, He Y, Smith A et al (2019) Cdkn2a (Arf) loss drives NF1-associated atypical neurofibroma and malignant transformation. Hum Mol Genet 28:2752–2762. https://doi.org/10.1093/hmg/ddz095

Rodriguez FJ, Folpe AL, Giannini C, Perry A (2012) Pathology of peripheral nerve sheath tumors: diagnostic overview and update on selected diagnostic problems. Acta Neuropathol 123:295–319. https://doi.org/10.1007/s00401-012-0954-z

Röhrich M, Koelsche C, Schrimpf D et al (2016) Methylation-based classification of benign and malignant peripheral nerve sheath tumors. Acta Neuropathol 131:877–887. https://doi.org/10.1007/s00401-016-1540-6

Schaefer IM, Fletcher CDM, Hornick JL (2016) Loss of H3K27 trimethylation distinguishes malignant peripheral nerve sheath tumors from histologic mimics. Mod Pathol 29:4–13. https://doi.org/10.1038/modpathol.2015.134

Sohier P, Luscan A, Lloyd A et al (2017) Confirmation of mutation landscape of NF1-associated malignant peripheral nerve sheath tumors. Genes Chromosom Cancer 56:421–426. https://doi.org/10.1002/gcc.22446

Talevich E, Shain AH, Botton T, Bastian BC (2016) CNVkit: genome-wide copy number detection and visualization from targeted DNA sequencing. PLOS Comput Biol 12:e1004873. https://doi.org/10.1371/journal.pcbi.1004873

Uusitalo E, Rantanen M, Kallionpää RA et al (2016) Distinctive cancer associations in patients with neurofibromatosis type 1. J Clin Oncol 34:1978–1986. https://doi.org/10.1200/JCO.2015.65.3576

Wagner V, Gil J (2020) Senescence as a therapeutically relevant response to CDK4/6 inhibitors. Oncogene 39:5165–5176. https://doi.org/10.1038/s41388-020-1354-9

Wang K, Li M, Hakonarson H (2010) ANNOVAR: functional annotation of genetic variants from high-throughput sequencing data. Nucleic Acids Res 38:e164–e164. https://doi.org/10.1093/nar/gkq603

Wong WW, Hirose T, Scheithauer BW et al (1998) Malignant peripheral nerve sheath tumor: analysis of treatment outcome. Int J Radiat Oncol Biol Phys 42:351–360. https://doi.org/10.1016/s0360-3016(98)00223-5

Zhang M, Wang Y, Jones S et al (2014) Somatic mutations of SUZ12 in malignant peripheral nerve sheath tumors. Nat Genet 46:1170–1172. https://doi.org/10.1038/ng.3116